Resonantly accelerated electrons from a tightly focused laser beam

O. Klimo[1,2], D. Kumar[2], J. Limpouch[1], S. Weber[2]

[1] *FNSPE, Czech Technical University in Prague, 11519 Prague, Czech Republic*

[2] *Institute of Physics of the ASCR, ELI-Beamlines, 18221 Prague, Czech Republic*

One of the most promising techniques to enhance focused laser intensities is to tightly focus the beam using an ellipsoidal plasma mirror. It has been successfully employed to obtain sub-μm spot size [1] resulting in an order of magnitude increase in focused intensity in comparison with a typical spot size of about 4 μm obtained with f/3 off axis parabolic mirror. The tightly focused laser beam is not purely transverse but it also includes non-negligible longitudinal field components, which modify the laser target interaction process. In particular the longitudinal electric field is very important at the periphery of the focal spot. This paper describes the role of this longitudinal field component in laser absorption and hot electron generation on a surface of an overdense plasma target using two-dimensional Particle-in-Cell (PIC) simulations.

The strength of the longitudinal electric field can be estimated using the Gauss's law for the electric field in vacuum and approximating the transverse field component as

$$E_y = E_{y0}\sin(k_0 x)\exp\left(-\frac{y^2}{w_0^2}\right) . \tag{1}$$

The resulting longitudinal field is

$$E_x = \frac{2yE_{y0}}{k_0 w_0^2}\cos(k_0 x)\exp\left(-\frac{y^2}{w_0^2}\right) . \tag{2}$$

The amplitude of this field is about $\simeq 0.14\lambda_0/w_0\times$ smaller than that of the transverse field (E_{y0}) at the periphery of the focal spot ($y = w_0/\sqrt{2}$), where the E_x field is the strongest. The wavenumber of the wave is denoted $k_0 = 2\pi/\lambda_0$, where λ_0 is the laser wavelength. The longitudinal electric field (2) has a strong impact on laser absorption process in particular when $w_0 \leq \lambda_0$. Note that the field has a different phase on each side of the focal spot and it is phase shifted by $\pi/2$ with respect to the transverse field.

Electron dynamics and hot electron generation in the field of a tightly focused laser beam is demonstrated using PIC simulations in Fig. 1. The results are obtained using a modified version of the code EPOCH [2] in 2D geometry with the tight focusing implemented using the algorithm [3]. The laser beam parameters used are: $\lambda_0 = 1\mu m$, laser intensity $I_0 = 10^{21}$ W/cm^2, Gaussian pulse duration 30 fs FWHM, $w_0 = 0.6\lambda_0$, p-polarization (electric field in the simulation plane), normal incidence. The parameters used for the target are: free electron density

560 n_c, where n_c is the critical density ($n_c = \omega_0^2 \varepsilon_0 m_e / e^2$, ω_0 is the frequency of the laser wave, ε_0 is the vacuum permittivity and m_e a e are the electron mass and charge), immobile ions, target thickness 2 μm and step-like density profile.

Fig. 1 presents the electron bunch dynamics during a half laser period around the time when the peak intensity of the laser pulse reaches the target. The laser wave forms a standing wave in front of the target with the transverse electric field node and the antinode of the magnetic field and the longitudinal electric field at the surface of the target. The process of electron acceleration always starts short time after the magnetic field reaches its minimum (for $y > 0$) or maximum (for $y < 0$) during the laser cycle. At this time, the balance between the radiation pressure due to the $\mathbf{j} \times \mathbf{B}$ force, the restoring electrostatic force due to charge separation and the longitudinal electric field of the laser wave is violated. It results in pulling a very dense bunch of electrons from the target surface into the vacuum on one side of the focal spot (as seen in Fig. 1 upper row), while the electrons are pushed even more into the target on the other side.

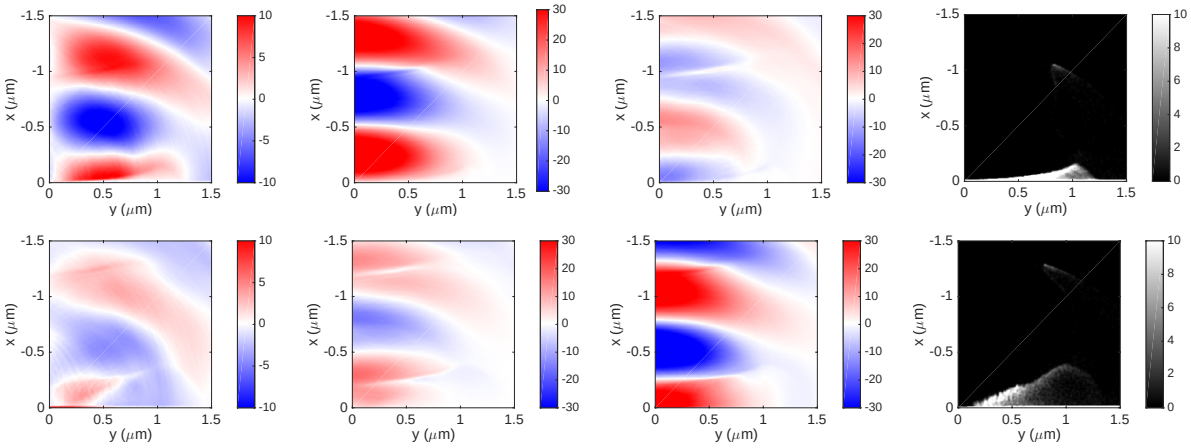

Figure 1: *The electric and magnetic fields (normalized by $m_e \omega_0 c/e$ and $m_e \omega_0 / e$ respectively) and the density of electrons (in units of n_c). The laser pulse is incident from the top and the target surface is located at $x = 0$. From left to right E_x, E_y, B_z and n_e. Time difference between the top and the bottom row is quarter period.*

A quarter period later (Fig. 1, bottom row), the polarity of the magnetic the longitudinal electric fields are reversed and thus they are accelerating the bunch of electrons back into the target. The longitudinal field of the laser wave has two important effects on the acceleration process. The strength of this field determines the charge of the bunch and also how far the electrons are pulled from the target surface into vacuum. Even though, most of the energy gain of electrons is from the transverse electric field in front of the target, the longitudinal field determines how close these electrons may get to the transverse electric field antinode and thus how much energy they gain.

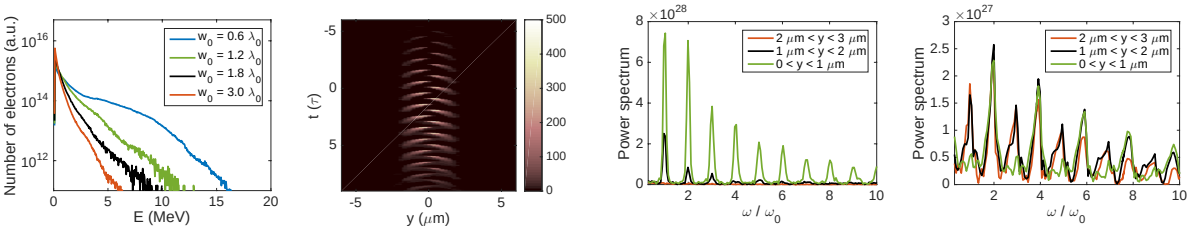

Figure 2: *(left) Comparison of the electron energy spectrum from PIC simulations in dependance on the waist of the focused beam. The spectrum shows electrons recorded at the rear side of the target during the whole simulation. (second from left) The density of hot electrons with energy* > 1 *MeV when they are crossing the rear side of the target into vacuum in arb. units for* $w_0 = 0.6\lambda_0$*. Time is measured in laser periods and 0 corresponds to the interaction of the peak laser field with the target. (second from right, right) The Fourier transform of the density of hot electrons crossing the rear side of the target into vacuum. The waist of the focused beam is* $0.6\lambda_0$ *(second from right) and* $3\lambda_0$ *(right). The y coordinate gives the distance from the laser axis where the signal is recorded at the rear side of the target.*

The effect of the longitudinal field component on the overall electron acceleration process is demonstrated in Fig. 2 in the electron energy spectrum. The parameters of the PIC simulations are the same like in Fig. 1 with exception of the waist of the focused laser beam. The spectrum shows that the number of hot electrons, the hot electron temperature and the cut-off energy increase with decreasing the waist. The number of accelerated electrons depends approximately linearly on the amplitude of the longitudinal field at the focal spot periphery, so it scales approximately like w_0^{-1}. However, as the temperature of hot electrons also increases with decreasing the waist, the efficiency of absorption into hot electrons shows a superlinear scaling.

Hot electrons with energy above 1 MeV are recorded when crossing the rear surface of the 2 μm thick target into vacuum with temporal and spatial resolution. From these data, we can reconstruct the spatio-temporal distribution of their density at the rear side, which is plotted in Fig. 2 second panel from the left for the case $w_0 = 0.6\lambda_0$. The figure clearly shows dense bunches of hot electrons accelerated once per laser period on each side of the focal spot phase shifted by half period comparing the $y < 0$ and $y > 0$ parts. This confirms our interpretation of the influence of the longitudinal electric field, which contributes to electron acceleration on one side of the focal spot while inhibiting electron acceleration on the other side at the same time.

Finally, we make the Fourier transform of the density of hot electrons recorded at the rear side of the target as this should be related to the coherent transition radiation (CTR) [4], which may be measured in experiment. This Fourier transform is plotted in Fig. 2 (two panels on the right side) for $w_0 = 0.6$ and $3\lambda_0$. The figures demonstrate that the dominant frequency of hot electron arrival at the rear side for the tightly focused laser beam is ω_0. If the Fourier transform is taken

on the axis, a strong $2\omega_0$ component is also present together with many harmonics. This is due to the overlap of the hot electron bunches from both sides of the the focal spot ($y < 0$ and $y > 0$) in this region. However, moving away from the laser axis, the signal with the frequency ω_0 largely dominates. This is not the case of the spectrum calculated for the larger spot size $w_0 = 3\lambda_0$ where the acceleration is due to the $\mathbf{j} \times \mathbf{B}$ Lorentz force with only a negligible contribution of the longitudinal field. In this case, the bunches of hot electrons are accelerated from the whole focal spot area two times per laser period. The spectrum thus shows the dominant frequency $2\omega_0$. There is also a peak at the frequency ω_0 for $y > 1\mu$m in this spectrum but it is always much weaker than the dominant peak at frequency $2\omega_0$.

In conclusion, the electron acceleration process is studied in this paper using PIC simulations with the code EPOCH under tight focusing conditions. The electrons are first pulled from the target surface by the longitudinal component of the laser electric field. In the next phase, the electrons are accelerated by the transverse laser electric field and finally, the $\mathbf{v} \times \mathbf{B}$ Lorentz force accelerates these electrons into the target where they propagate further ballistically. As the longitudinal field has an opposite phase on both sides of the focal spot, the bunches originating from this process are phase shifted by half a laser period and they propagate in different directions because of the wavefront curvature. This opens the possibility to diagnose the absorption process with coherent transition radiation at the rear side of the target, where the bunches arrive at a rate given by the laser frequency (ω_0) in contrast with the simple $\mathbf{j} \times \mathbf{B}$ heating process dominating for less tightly focused laser beams where the contribution of the longitudinal electric field is negligible and the rate is given by $2\omega_0$. The results presented in this paper were obtained in simulations with immobile ions. Ion mobility does not influence the absorption process qualitatively, but the difference in absorption efficiency is not so big in simulations with mobile ions.

Acknowledgments: This work is supported by European Regional Development Funds - projects "CAAS" (No. CZ.02.1.01/0.0/0.0/16_019/0000778), "ELITAS" (ELI Tools for Advanced Simulation) CZ.02.1.01/0.0/0.0/16_013/0001793, and "HiFI" (High-Field Initiative) CZ.02.1.01/0.0/0.0/15003/0000449 and by the Czech Science Foundation project 18-09560S.

References

[1] M. Nakatsutsumi, A. Kon, S. Buffechoux *et al.*, Opt. Lett. **35**, 2314–2316 (2010)

[2] T. D. Arber, K. Bennett, C. S. Brady *et al.*, Plasma Phys. Control. Fusion **57**, 1–26 (2015)

[3] I. Thiele, S. Skupin and R. Nuter, J. Comput. Phys. **321**, 1110–1119 (2016)

[4] C. Bellei, J. R. Davies, P. K. Chauhan and Z. Najmudin, Plasma Phys. Control. Fusion **54**, 035011 (2012)